A Hybrid Polynomial Stall Model for the Longitudinal Dynamics of a UAV

Vincent Guibert, Jean-Philippe Condomines, Mathieu Brunot, Jean-Marc Biannic, Murat Bronz

A Hybrid Polynomial Stall Model for the Longitudinal Dynamics of a UAV

Vincent Guibert[1], Jean-Philippe Condomines[1], Mathieu Brunot[2], Jean-Marc Biannic[2] and Murat Bronz[1]

***Abstract*— Modeling the longitudinal dynamics of a fixed-wing unmanned aerial vehicle (UAV) at high angles of attack is not an easy task. Indeed, when the airplane approaches stall, non-linear effects appear, including transient behaviors and an aerodynamic hysteresis. Although some models are present in the literature to address these aspects, they are usually aerodynamics-based and often too complex for analysis and control applications. Therefore, this paper presents a new hybrid polynomial formulation for the modeling of the aerodynamic coefficients. In addition, a Linearly Constrained Least Squares (LCLS) process guaranteeing continuity at the mode transitions is proposed for the identification of the model. The Hybrid Polynomial Stall Model (HPSM) is finally identified on experimental wind tunnel data, showcasing its ability to accurately predict a UAV's dynamics.**

I. Introduction

Modeling the dynamics of an airplane is not a simple and straightforward task, as it behaves in an unsteady and non-linear way. In particular, above a so-called "stall angle of attack" the air flow above the wings detaches, which in turn impacts the airplane's behavior [1]. Moreover, this aerodynamic phenomenon presents a hysteresis, as the lift does not vary with the angle of attack in the same fashion for positive and negative angle of attack rates [2]. This hysteresis has already been studied in several works for full-scale airplanes [3] or a single wing [4]. However, no analytical solution is known and Computational Fluid Dynamics (CFD) calculations are extremely resource-heavy both in term of computation power and user knowledge [5]. In addition, in-flight measurements are rare due to the risks involved with flying an aircraft outside of its designated flight envelope.

Fixed-wing Unmanned Aerial Vehicles (UAVs) suffer from this same issue as their design is extremely close to that of full-scale airplanes. They however typically have lower Reynolds numbers in the 1e5–1e6 range compared to airplanes which have Reynolds number in the 1e7–1e8 range. Their dynamic response might hence be different as the air flow around them is expected to behave differently. A model able to accurately predict their dynamics on a wide flight envelope could therefore prove valuable for the ongoing certification and integration into urban and civil airspace of UAVs, as is for instance the case for the European Union [6]. Possible applications include the certification of a UAV's control law and providing with an accurate prediction tool including at-stall and post-stall dynamics for advanced control. In particular, it could pave the way for robust stall recovery controllers, lowering the risks for UAVs, the other users of the airspace, ground infrastructures, and people.

Modeling the dynamics of a UAV is an ongoing subject of research. Even though the community mostly agrees on a "linear" representation for low angles of attack, no consensus exists for high angles of attack modeling. In fact, many authors have presented many models, originating from very different solutions. For instance, [7] proposed to solve numerically the Navier-Stokes equations, while [4] uses semi-empirical models. Others have proposed fully data-driven models such as locally weighted projection regression [8] or splines [9]. However, while splines present today a powerful tool for accurate and smooth interpolation [10], their complexity make them difficult to use for functional analysis of trim conditions and stable sets. All those models have however already been compared to one another by various authors in the literature (e.g. [1], [11]) and it would be both redundant and impractical to list them all here. Moreover, high-fidelity models often require hard to obtain data, such as the flow separation point, which is usually not available in flight.

On the other hand, piecewise polynomials have been used for various applications due to their simple nature. Examples are numerous and include various fields such as healthcare [12] or biology [13]. They have also been used for the modeling of dynamical systems, including airborne object [14]. Reference [15], for instance, proposed a formulation dependent on the Mach number of projectiles. More notably, [16] proposed a two-pieced polynomial for the aerodynamic coefficients dependent on the angle of attack. The authors however chose to focus on the location of stable sets and the control of the airplane in deep stall, putting aside preceding stall effects like the aerodynamic hysteresis. Finally, previous work obtained results with a four-pieced polynomial for the modeling of the lift coefficient of a single wing, with a special focus on the aerodynamic hysteresis [17]. With the exception of [16], however, all results above are restricted to one-dimensional polynomials. In addition, the joints are often supposed known beforehand, although some authors proposed optimization methods for their estimation [12], [17].

Following this review, this paper presents an extension of

This work was supported by the Defense Innovation Agency (AID) of the French Ministry of Defense (research project CONCORDE N° 2019 65 0090004707501)

[1]Vincent Guibert, Jean-Philippe Condomines and Murat Bronz are with ENAC, Université de Toulouse, 31400 Toulouse, France {vincent.guibert, jean-philippe.condomines, murat.bronz} @enac.fr

[2]Mathieu Brunot and Jean-Marc Biannic are with the Department of Systems and Information Processing, ONERA – The French Aerospace, 31400 Toulouse, France {mathieu.brunot, jean-marc.biannic} @onera.fr

the PwPM method from [17] from the lift coefficient of a single wing to the longitudinal dynamics of a more realistic model of a UAV. This new model is hybrid polynomial and defined for the three degrees of freedom longitudinal dynamics of a fixed-wing UAV. It showcases an emphasis on the dynamic component of stall and in particular the aerodynamic hysteresis while retaining the simple formulation best suited for control and analysis applications. In addition, a Linearly Constrained Least Squares (LCLS) process guaranteeing continuity at the mode transitions is proposed for the identification of the model.

After introducing in Section II the piecewise polynomial modeling of an airplane's dynamics and hybrid modeling, this paper presents the proposed Hybrid Polynomial Stall Model (HPSM) in Section III, including its Finite State Machine (FSM) and the polynomials themselves. Section IV presents the identification process in the Linearly Constrained Least Squares (LCLS) sense and is followed by the application of this model to experimental data in Section V.

II. High angles of attack polynomial modeling

A. Longitudinal dynamics modeling

The longitudinal behavior of an airplane is modeled in its wind axis by the following set of four equations:

$$\begin{aligned} \dot{V} &= \frac{1}{m}\left(T\cos\alpha - \bar{q}SC_D\right) - g\sin\gamma \\ \dot{\alpha} &= q + \frac{1}{mV}\left(-T\sin\alpha - \bar{q}SC_L\right) + \frac{g}{V}\cos\gamma \\ \dot{q} &= \frac{1}{I_{yy}}\left(\bar{q}SlC_m\right) \\ \dot{\gamma} &= q - \dot{\alpha} \end{aligned} \tag{1}$$

where the aircraft's state is given by its airspeed V, its angle of attack α, its pitch rate q and its flight path angle γ. The commands are the thrust force T, supposed applied at the airplane's center of mass and in direction of the forward axis in its body frame, and the elevator deflection angle δ. This last command does not appear directly in (1) but it acts on the three aerodynamic coefficients C_L, C_D and C_m respectively for the lift force, drag force, and pitch moment. In addition, the airplane has a mass m, a moment of inertia about its pitch axis I_{yy}, a reference area S and a reference length l. Finally, $\bar{q} = \frac{1}{2}\rho V^2$ is the dynamic pressure, ρ the surrounding air density and g the local gravitation field acceleration.

In this formulation, the three aerodynamic coefficients C_L, C_D and C_m are of prime importance because they house all the different effects that can act on the airplane, including non-linear ones. Being able to model these coefficients is therefore akin to modeling the whole of the dynamics of the airplane. In addition to the elevator deflection angle, as already stated, they are function of a wide range of parameters, including the airplane's flight configuration (gears and flaps position, etc.) and its aerodynamic one (angle of attack, its rate, etc.). For low angles of attack, the usual flight configuration of airplanes, these coefficients can be reasonably approximated by linear relations and this strategy is the one used with great success on most UAVs [18]. However, when the angle of attack becomes too high this assumption is no longer valid, and not taking into account this change can pose a threat to the controllability of the airplane. A better model for high angles of attack is therefore paramount both for performance and security.

B. Piecewise polynomial modeling

As was presented in the introduction, the literature is abundant on the subject of high angles of attack dynamics modeling. Most models are however too complex for the easy analysis of the airplane's stability or on-board predictions, preventing their use in model-based control laws. In addition, they can be hard to identify although recent advances (in particular in Machine Learning) have opened new ways to do so [19]. That is why some authors have proposed specific tools to approximate these phenomena with more standard polynomial or rational expressions which can be easily converted into a Linear Fractional Transformation (LFT) format, this last format being well suited to analysis and control design applications [20].

In addition, polynomials have several more advantages which make them well-suited for these tasks. Firstly, they are easy and quick to evaluate. Secondly, they are easily differentiated and their derivatives remain polynomials, providing with fast access to the Jacobian, which is a useful property, in particular for analysis applications. Lastly, their formulation can be rewritten as the scalar product of a vector of monomials $\mu(\boldsymbol{x}) \in \mathbb{R}^\delta$ and the vector of their coefficients $\boldsymbol{\theta} \in \mathbb{R}^\delta$:

$$\hat{f}(\boldsymbol{x}) = \langle \mu(\boldsymbol{x}), \boldsymbol{\theta} \rangle = \mu(\boldsymbol{x})^\intercal \boldsymbol{\theta} \tag{2}$$

This last property is particularly interesting in the case of the Least Squares (LS) identification of such a model, as it allows an analytical solution as was shown in previous work [17].

A monobloc polynomial function can however be unable to accurately approximate some systems. A wide range of variations in the system state function would require prohibitively high polynomial degrees, impairing the identification process. In addition, some systems present with vastly different behaviors, sometimes even for seemingly identical situations as is the case during hysteresis phenomena. Hence, authors have proposed piecewise polynomial formulations [16]. In this formulation, the state space $\mathcal{X} \subset \mathbb{R}^n$ is partitioned into subspaces and for each, the model is expressed independently:

$$\hat{f}(\boldsymbol{x}) = \begin{cases} \hat{f}_1(\boldsymbol{x}) = \mu_1(\boldsymbol{x})^\intercal \boldsymbol{\theta_1} & \text{if } \boldsymbol{x} \in \mathcal{X}_1 \\ \hat{f}_2(\boldsymbol{x}) = \mu_2(\boldsymbol{x})^\intercal \boldsymbol{\theta_2} & \text{if } \boldsymbol{x} \in \mathcal{X}_2 \\ \quad\vdots & \\ \hat{f}_N(\boldsymbol{x}) = \mu_N(\boldsymbol{x})^\intercal \boldsymbol{\theta_N} & \text{if } \boldsymbol{x} \in \mathcal{X}_N \end{cases} \tag{3}$$

where the different state subspaces are denoted $\mathcal{X}_i$. They must form a partition of the state space and as such respect the following two relations:

$$\bigcup_i \mathcal{X}_i = \mathcal{X} \qquad \text{and} \qquad \forall i \neq j,\ \mathcal{X}_i \cap \mathcal{X}_j = \emptyset \tag{4}$$

This form trades the complexity of a high-degree monobloc polynomial for the added overhead of having to distribute the abscissae into the different subspaces. However, each polynomial is expected to be a lot simpler for the same precision, provided the subspaces $\mathcal{X}_i$ were chosen adequately. Unfortunately, some properties of the monobloc polynomial are lost, most notably the continuity at the intersection of each two subspaces. If this is required of the model, this condition has to be specified as a constraint during the identification process, which can complexify this process. Once again, however, previous works have shown that in the case where these constraints are linear in the polynomial coefficients (which is the case in most usual constraints thanks to the polynomial formulation) an analytical solution can still be found [17].

C. Hybrid polynomial modeling

Hybrid models are the combination of a continuous state model and a discrete state controlled by a Finite State Machine (FSM) [21]. This configuration allows the definition of a distinct model for each discrete state, which therefore acts as the mode of the system. Their formal definition is given as:

$$\hat{f}(\boldsymbol{x}) = \begin{cases} \hat{f}_1(\boldsymbol{x}) & \text{if } i = s_1 \\ \hat{f}_2(\boldsymbol{x}) & \text{if } i = s_2 \\ \quad \vdots & \\ \hat{f}_N(\boldsymbol{x}) & \text{if } i = s_N \end{cases} \tag{5}$$

where $i \in \{s_1, s_2, \cdots, s_N\} = \mathcal{S}$ is the mode.

The changes in mode are handled by the FSM using transition conditions. Without loss of generality, we will take here conditions of the shape

$$g_{j\to k}(\boldsymbol{x}) = 0 \tag{6}$$

where $g_{j\to k} : \mathbb{R}^n \to \mathbb{R}$ is a transition helper function used in the transition from mode j to mode k. In addition, these transition helper functions will be taken as positive before the transition and therefore negative after.

Following from the definition above, piecewise polynomial systems are in fact a special case of hybrid polynomial ones, where the mode $i(t)$ is given as the index of the sole subspace $\mathcal{X}_i \mid \boldsymbol{x}(t) \in \mathcal{X}_i$.

Relaxing the previous model to a hybrid one therefore allows a greater flexibility, once again at some added complexity. Mostly, improvements will be made for systems presenting with a hysteresis, where for the same abscissa, there can be two different behaviors depending on the trajectory history.

III. Hybrid Polynomial Stall Model

Following from the definitions above, we propose to model the relation between the aerodynamic coefficients and their abscissae using such a hybrid polynomial model.

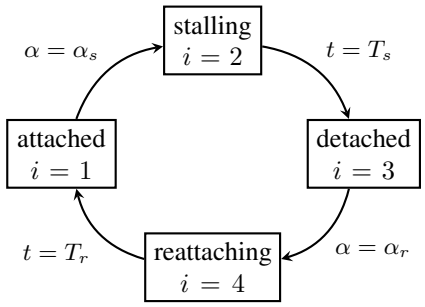

Fig. 1. The mode's Finite State Machine for the proposed model.

A. Modes

The first thing to do is therefore to select the different modes. Based on *a priori* knowledge from the literature and experimental data (e.g. [17]), four distinct behaviors were extracted:

- Two regular modes, respectively for when the air flow is attached to the wings and when it is detached.
- Two transient modes, which are limited in time and represent the morphing from one of the regular mode to the other. They correspond to the airplane's dynamics when the flow separation point moves along the wing chord.

The choice of the two regular modes is pretty straightforward, as we expect the UAV's dynamic to be different below and above stall due to the difference in air flow behavior, giving rise to this study. The choice of two transient modes however is less common. Several authors have indeed ignored this aspect, choosing to consider them instantaneous (e.g. [2]). In the case of dynamic stall however, they hold an important part of the airplane's behavior. In addition, although they only take a few tenth of seconds, this time is sufficient for a UAV to span a distance of several times its own length.

Finally, not all modes are reachable from all others. In fact, all modes have a single incoming neighbor and another single outgoing one. This defines the mandatory cycle an airplane has to follow if it were to come back to an attached air flow after stalling: attached air flow $\to$ stalling air flow $\to$ detached air flow $\to$ reattaching air flow $\to$ attached air flow. This behavior of the mode's FSM is represented as the multidigraph in Fig. 1.

B. Transitions

The transitions from one mode to another are defined depending on the initial mode:

- A time-insensitive (regular) mode (attached or detached) is left when the airplane crosses a specific angle of attack: α_s for stall and α_r for flow reattachment.
- Time-sensitive modes are left after a given duration, when the transient effects due to the air flow's detachment or reattachment have subsided. The duration of the stalling mode is T_s and that of the reattachment one is T_r.

In the first case, the two transition angles of attack can be quite hard to define. The value of the stall angle of attack α_s, for instance, is not fixed as several authors have noted that stall appears to be delayed for higher angle of attack rates [3], [4]. This phenomenon is known as dynamic stall. There however isn't an agreed-upon formulation for this value. Based on the experimental data presented below, it however appeared that it could be approximated by a linear function in the angle of attack rate $\dot{\alpha}$, hence the selected value:

$$\alpha_s = \alpha_s^\circ + k_s \cdot \dot{\alpha}, \quad \dot{\alpha} \in [0, +\infty) \tag{7}$$

where α_s° is the steady case stall angle of attack and k_s the rate proportionality coefficient. Stall is however not possible for negative angle of attack rates, as the angle of attack is decreasing. Hence the positivity condition on $\dot{\alpha}$. The opposite reasoning holds for the reattachment angle of attack. Therefore, we introduce the reattachment angle of attack α_r for negative angle of attack rates:

$$\alpha_r = \alpha_r^\circ + k_r \cdot \dot{\alpha}, \quad \dot{\alpha} \in (-\infty, 0[\tag{8}$$

Finally, the transition helper functions can be easily defined following all those definitions as:

$$\begin{aligned} g_{1\to2}(\alpha, \dot{\alpha}) &= \alpha_s^\circ + k_s \cdot \dot{\alpha} - \alpha \\ g_{2\to3}(t) &= T_s - t \\ g_{3\to4}(\alpha, \dot{\alpha}) &= \alpha - \alpha_r^\circ - k_r \cdot \dot{\alpha} \\ g_{4\to1}(t) &= T_r - t \end{aligned} \tag{9}$$

where the time t is the time since the entrance into the corresponding mode. It can be seen that the $\dot{\alpha}$ positivity (resp. negativity) condition for $g_{1\to2}$ (resp. $g_{3\to4}$) has been dropped, slightly changing the definitions from above. It is however not an issue since the case where the angle of attack reaches the stall angle of attack α_s with a negative rate is not expected to occur in-flight. The same is true with a positive rate and the reattachment angle of attack α_r.

C. Polynomials

Finally, the polynomials themselves must be defined. This is done by choosing the abscissae and the monomials to be used in each mode.

At this point, some assumptions must be made and we will consider the airplane to be in a clean configuration (no flaps, gears up, etc.). The aerodynamic coefficients will henceforth be considered dependent only on the three aerodynamic abscissae: the angle of attack α, its rate $\dot{\alpha}$ and the elevator deflection angle δ. In addition, the time spent since the entrance into the current mode, t, will be appended for the two transient modes.

$$\boldsymbol{x} = \begin{bmatrix} \alpha & \dot{\alpha} & \delta & t \end{bmatrix}^\intercal \tag{10}$$

Considering the monomials, we choose to use for all modes all available combinations of single-variable monomials up to a given degree:

$$\mu_i(\boldsymbol{x}) = \begin{bmatrix} 1 & \alpha & \dot{\alpha} & \alpha\dot{\alpha} & \cdots & \alpha^{\nu_\alpha^i}\dot{\alpha}^{\nu_{\dot{\alpha}}^i}\delta^{\nu_\delta^i}t^{\nu_t^i} \end{bmatrix}^\intercal \tag{11}$$

where the different natural integers $\nu_{\boldsymbol{x}_j}^i$ are the maximum degrees respective to each of the abscissae. This formulation gives a total number of monomials for each mode as

$$\nu_i = \prod_j \left(\nu_{\boldsymbol{x}_j}^i + 1\right) \tag{12}$$

and a total number of regressors for each aerodynamic coefficients

$$\nu = \sum_{i=1}^{N} \nu_i = \sum_{i=1}^{N} \left(\prod_j \left(\nu_{\boldsymbol{x}_j}^i + 1\right) \right) \tag{13}$$

These maximum degrees were chosen by iterating over the model, starting from an initial guess for all modes $\nu_\alpha^i = \nu_{\dot{\alpha}}^i = \nu_\delta^i = 1$ and $\nu_t^i = 0$ for the time-insensitive modes and $\nu_t^i = 3$ for the transient ones. At each step, the Akaike Information Criterion (AIC) [22] was computed and compared to those of the same model with a single maximal degree modified to be one greater or one lesser. In the Least Squares (LS) sense, the AIC value is given as:

$$\mathrm{AIC} = 2\nu + N_{meas} \ln(\mathrm{RSS}) \tag{14}$$

where N_{meas} is the number of measurements and $\mathrm{RSS} = \sum_{k=1}^{N_{meas}} \left(y_k - \hat{f}(\boldsymbol{x_k})\right)^2$ the residual sum of squares on the measurements. The best trade off between model complexity and precision as given by the minimum of AIC was then selected as the new model. The final values are given in Table I.

It is noted that the identical degrees on each modes are not a design requirement but rather the result of the AIC minimization method used.

In the end, the lift coefficient is modeled using $\nu_L = 320$ polynomial coefficients, the drag one using $\nu_D = 240$ coefficients and the pitch moment coefficient using $\nu_m = 240$ regressors.

D. Complete model

Finally, the complete Hybrid Polynomial Stall Model (HPSM) is given as the combination of the FSM described by both the multidigraph from Fig. 1 and the transition helper functions from (9) ; and the polynomial degrees from Table I.

IV. Identification

Before moving on to the experimental results, we must ensure that the identification process from [17] can be used despite the update of the model.

The difference between the model PwPM model from [17] and the new HPSM is the way in which abscissae are linked to their corresponding polynomials. However, once that is done, the same variables can be introduced. Namely, the vector of regressors

$$\phi(\boldsymbol{x}) = \begin{bmatrix} \tau(i=1)\cdot\mu_1(\boldsymbol{x}) \\ \tau(i=2)\cdot\mu_2(\boldsymbol{x}) \\ \vdots \\ \tau(i=N)\cdot\mu_N(\boldsymbol{x}) \end{bmatrix} \tag{15}$$

TABLE I

MAXIMUM DEGREE OF EACH OF THE AERODYNAMIC COEFFICIENT POLYNOMIALS WITH RESPECT TO EACH OF THE ABSCISSAE.

	C_L				C_D				C_m			
	$i=1$	$i=2$	$i=3$	$i=4$	$i=1$	$i=2$	$i=3$	$i=4$	$i=1$	$i=2$	$i=3$	$i=4$
α	3	2	3	2	3	2	3	2	3	2	3	2
$\dot{\alpha}$	3	3	3	3	3	2	3	2	3	2	3	2
δ	1	1	1	1	1	1	1	1	1	1	1	1
t	0	3	0	3	0	3	0	3	0	3	0	3

where the activation function τ equals one when its condition is true and zero otherwise:

$$\tau(\text{condition}) = \begin{cases} 1 & \text{if the condition holds} \\ 0 & \text{otherwise} \end{cases} \tag{16}$$

and the corresponding vector of model coefficients

$$\boldsymbol{\theta} = \begin{bmatrix} \boldsymbol{\theta_1}^\intercal & \boldsymbol{\theta_2}^\intercal & \cdots & \boldsymbol{\theta_N}^\intercal \end{bmatrix}^\intercal \tag{17}$$

The model output is then rewritten in the very same way using the scalar product

$$\hat{f}(\boldsymbol{x}) = \langle \phi(\boldsymbol{x}), \boldsymbol{\theta} \rangle = \phi(\boldsymbol{x})^\intercal \boldsymbol{\theta} \tag{18}$$

A. Constraints

Recall however that the hybrid formalism used in the new HPSM does not guarantee the continuity when changing mode. Yet, the aerodynamic coefficients are expected to be continuous over the whole domain, including at stall and reattachment. A constraint must therefore be added as previously stated to the identification process to ensure this property of the identified model.

Such conditions are quite complex to express mathematically on the different transitions. Fortunately, there is no need to do so thanks to the polynomial formulation of the model. In order to show this, let us consider the continuity between two modes j and k. This constraint can be written as:

$$\forall \boldsymbol{x} \mid g_{j\to k}(\boldsymbol{x}) = 0, \quad \phi_{i=j}(\boldsymbol{x})^\intercal \boldsymbol{\theta} = \phi_{i=k}(\boldsymbol{x})^\intercal \boldsymbol{\theta} \tag{19}$$

where the vectors of regressors, taken from (18), are evaluated assuming the mode is respectively j and k.

For conciseness, let us introduce a new regressors vector $\phi_{j-k}(\boldsymbol{x}) = \phi_{i=j}(\boldsymbol{x}) - \phi_{i=k}(\boldsymbol{x})$ such that (19) becomes

$$\forall \boldsymbol{x} \in \ker g_{j\to k}, \quad \phi_{j-k}(\boldsymbol{x})^\intercal \boldsymbol{\theta} = 0 \tag{20}$$

This new vector $\phi_{j-k}(\boldsymbol{x})$ controls which and how the model coefficients will be impacted by the constraint. However, not all its regressors are linearly independent, either because of the monomials for modes j and k themselves (for instance if both have the same monomial, these rows will be opposite to one another and therefore not independent) or because of implicit relationships inherited from the subspace $\ker g_{j\to k}$ (in the case of stall, for instance, the regressor α is a linear combination of the regressors 1 and $\dot{\alpha}$), leading to information being repeated. Therefore, if we have a set of $m_{j\to k}$ points $\{\boldsymbol{x_1^{j\to k}}, \boldsymbol{x_2^{j\to k}}, \cdots, \boldsymbol{x_{m_{j\to k}}^{j\to k}}\}$ in $\ker g_{j\to k}$ spanning all possible linearly independent regressors, the constraint from (19) on the subspace $\ker g_{j\to k}$ can be expressed as the following system of point equations:

$$\begin{cases} \phi_{j-k}(\boldsymbol{x_1^{j\to k}})^\intercal \boldsymbol{\theta} = 0 \\ \phi_{j-k}(\boldsymbol{x_2^{j\to k}})^\intercal \boldsymbol{\theta} = 0 \\ \vdots \\ \phi_{j-k}(\boldsymbol{x_{m_{j\to k}}^{j\to k}})^\intercal \boldsymbol{\theta} = 0 \end{cases} \tag{21}$$

Moreover, if there are exactly as many such points as there are linearly independent regressors in ϕ_{j-k}, there is no redundant information.

The value of $m_{j\to k}$ satisfying both conditions does not have a simple definition without an extensive knowledge of the regressors in ϕ_{j-k} and the transition function $g_{j\to k}$ kernel space. However, it is always bounded (worst case scenario, there is as many linearly independent regressors as there are non-null ones $m_{j\to k} = \nu_j + \nu_k$, with ν_j and ν_k the number of regressors for polynomials j and k respectively). It is therefore possible to draw randomly generated points in the subspace $\ker g_{j\to k}$ and remove all points which do not add information[1].

Concatenating system (21) into matrical form yields the matrix

$$\boldsymbol{C_{j\to k}} = \begin{bmatrix} \phi_{j-k}(\boldsymbol{x_1^{j\to k}})^\intercal \\ \phi_{j-k}(\boldsymbol{x_2^{j\to k}})^\intercal \\ \vdots \\ \phi_{j-k}(\boldsymbol{x_{m_{j\to k}}^{j\to k}})^\intercal \end{bmatrix} \tag{22}$$

which enables us to rewrite the constraint into the matrical form:

$$\boldsymbol{C_{j\to k}}\boldsymbol{\theta} = \boldsymbol{0} = \boldsymbol{d_{j\to k}} \tag{23}$$

where the constraint vector $\boldsymbol{d_{j\to k}}$ was introduced in order to generalize the results below.

As in [17], the same property holds for all usual constraints, including as continuity, tangency and specific value on any subspace. Hence, all the constraints can be once again written as linear combinations of the model coefficients:

$$\boldsymbol{C}\boldsymbol{\theta} = \boldsymbol{d} \tag{24}$$

where the matrix $\boldsymbol{C}$ collects all constraint matrices $\boldsymbol{C_{j\to k}}$ and the vector $\boldsymbol{d}$ all constraint vectors $\boldsymbol{d_{j\to k}}$.

[1] One has to be very careful however that all aspects of the kernel subspace are sufficiently represented by the randomly generated points in order not to miss any aspect. In particular, only points with positive (resp. negative) angle of attack rates must be selected for the stall (resp. reattachment) transition.

B. Linearly Constrained Least Squares

Finally, the identification problem is once again expressed as the Linearly Constrained Least Squares (LCLS) problem

$$\begin{aligned} \text{Find } \boldsymbol{\theta}^* = \arg\min_{\boldsymbol{\theta}} \frac{1}{2} [\boldsymbol{z} - \boldsymbol{\Phi}\boldsymbol{\theta}]^\intercal \boldsymbol{\Gamma} [\boldsymbol{z} - \boldsymbol{\Phi}\boldsymbol{\theta}] \\ \text{s.t.} \quad \boldsymbol{C}\boldsymbol{\theta}^* = \boldsymbol{d} \end{aligned} \tag{25}$$

where $\boldsymbol{z}$ is the vector of ordinate measurements, $\boldsymbol{\Phi}$ the matrix of regressors where each row is the vector of regressors for a new measurement, extrapolated from (18), and $\boldsymbol{\Gamma}$ a diagonal positive semi-definite matrix of measurement weights. As was the case for the constraint vector $\boldsymbol{d}$, this last variable was added in order to generalize the problem and in the application below, it was simply taken as the identity matrix $\boldsymbol{\Gamma} = \boldsymbol{I}$.

The solution to the LCLS problem is given using the Lagrange multipliers method as the solution of the Karush–Kuhn–Tucker (KKT) equation:

$$\begin{bmatrix} \boldsymbol{\Phi}^\intercal \boldsymbol{\Gamma} \boldsymbol{\Phi} & \boldsymbol{C}^\intercal \\ \boldsymbol{C} & \boldsymbol{0} \end{bmatrix} \begin{bmatrix} \boldsymbol{\theta}^* \\ \boldsymbol{\lambda}^* \end{bmatrix} = \begin{bmatrix} \boldsymbol{\Phi}^\intercal \boldsymbol{\Gamma} \boldsymbol{z} \\ \boldsymbol{d} \end{bmatrix} \tag{26}$$

where the $\boldsymbol{\lambda}^*$ are the optimal Lagrange multipliers. They are not required to be computed apart for verification purposes.

C. Optimization

The constraint matrix $\boldsymbol{C}$ can however only be built if the transition functions are exactly known. This is usually not the case in practice as they depend on a set of hyper-parameters which are not known beforehand. They must also be identified.

One of the strengths of the hybrid polynomial formulation is the analytical solution as was shown in the previous subsection. Another is that the optimal cost

$$J^* = \frac{1}{2} [\boldsymbol{z} - \boldsymbol{\Phi}\boldsymbol{\theta}^*]^\intercal \boldsymbol{\Gamma} [\boldsymbol{z} - \boldsymbol{\Phi}\boldsymbol{\theta}^*] \tag{27}$$

is continuous if continuity constraints have been appended for all neighboring polynomials. Under these conditions, a higher-level iterative optimization algorithm on the optimal cost J^* can be devised in order to find the best constraint hyper-parameters.

V. Experimental results

The HPS model was applied to experimental data.

A. Data Acquisition

A scale model representing the left half of a fixed-wing UAV was built as the combination of a main wing with profile NACA 0012, half wing span 500mm and chord 150mm ; and a monobloc elevator also with profile NACA 0012, with span 150mm and chord 60mm. This elevator was controllable and could take deflection angles in the $[0°, +20°]$ range. The model was able to rotate freely around its pitch axis at a point representing its center of mass arbitrarily set at 25% of its wing chord. It was installed left wing up so as to get no interaction with gravity into a WindShaper open wind tunnel capable of generating constant winds of up to 10m/s. The model was instrumented in order to provide with measurements for the aerodynamic force it experienced as well as its angle of attack, measured at its pivot.

During each experiment, the elevator deflection was set to $0°$ for a few seconds in order to ensure an initial null angle of attack. It was then maintained at a constant positive value δ_c for the remainder of the experiment (about 20s). Two different wind velocities V were tested: 7.5m/s and 10m/s, and four elevator deflection angles δ_c: $5°$, $10°$, $15°$ and $20°$.

All signals were sampled at approximately 100Hz in a non-uniform way due to inconsistent delays in the acquisition brought on by the hardware and softwares used. They were therefore re-sampled at exactly 100Hz using the Piecewise Cubic Hermite Interpolating Polynomial (PCHIP) interpolation method.

The campaign generated a set of 17,248 data points in the shape $(\alpha_k, \delta_k, L_k, D_k)$, where the subscripts k denote the measurement index and L and D are the lift force and the drag force respectively. The angle of attack measurements were then filtered twice using a second-order low-pass Butterworth filter (once forward and once backward) with a cutoff frequency of 5Hz. The resulting signal was then differentiated using a first order centered finite difference with an accuracy of 4 in order to numerically compute the angle of attack rate $\dot{\alpha}_k$. The pitch moment M_k was derived from the angle of attack acceleration, itself obtained similarly using a second order centered finite difference, also with an accuracy of 4.

Finally, the aerodynamic coefficients $C_{L,k}$, $C_{D,k}$ and $C_{m,k}$ were computed from the well-known equations

$$C_{L,k} = \frac{1}{\bar{q}S} L_k \qquad C_{D,k} = \frac{1}{\bar{q}S} D_k \qquad C_{m,k} = \frac{I_{yy}}{\bar{q}Sl} \ddot{\alpha}_k \tag{28}$$

to provide measurements for the model's desired output.

It is worth noting that the more noisy the angle of attack measurements are, the more important a proper setup of the Butterworth filters will be in order to provide accurate values for the numerically-derived variables $\dot{\alpha}$ and $\ddot{\alpha}$.

Before the fitting however, the three abscissae α, $\dot{\alpha}$ and δ were normalized linearly such that their means were 0 and their standard deviations 1.0.

$$\tilde{x}_{j,k} = \frac{x_{j,k} - \text{mean}(\boldsymbol{x_j})}{\text{std}(\boldsymbol{x_j})} \tag{29}$$

This was done in order to achieve a better condition number for the KKT matrix before its inversion.

In addition, 20% of measurements were chosen at random to serve as a validation dataset, while the remaining 80% were used for the fitting. These points were chosen at random because of the small number of experiments (8) where each was susceptible to hold unique information.

B. Optimization

After finding the model's maximum degrees using the methodology from Section III-C using an initial guess for the constraint hyper-parameters, these values were optimized based on our data.

TABLE II
GOODNESS OF FIT FOR EACH COEFFICIENT ON THE VALIDATION DATASET USING THE NRMSE METRIC.

Coefficient	C_L	C_D	C_m
Validation GoF	84.9%	78.1%	75.4%

To do so, we chose to apply a Random Optimization (RO) process [23]. This family of optimizers searches for a local minimum by nudging the previously-found best solution in a random direction in the hope that the new cost function evaluates to a lower value. Although this process is erratic, it has the advantage of not requiring the computation of a gradient vector. This is important in our case as this gradient is expensive to compute. In addition, numerical imprecisions could render gradient descent algorithms unstable.

The final parameters were found as follows: $\alpha_s^\circ = 15.8°$, $k_s = 54.6$ms, $\alpha_r^\circ = 13.0°$ and $k_r = -8.00$ms.

C. Results

The fitted polynomials are too complex to be given here, each having several hundred coefficients. The precision of their fitting can however be evaluated through the Goodness of Fit (GoF) of their predictions respective to the validation dataset. In this paper, we used the Normalized Root Mean Square Error (NRMSE) cost function in an effort to put into relation the error on the prediction and the measurement's own noise level. These results are given Table II.

These GoFs are firmly in the high seventies, with the lift one above eighty, showcasing the precision of the model's predictions.

To further reinforce this result, the model's predictions for two different experiments are given Fig. 2.

As can be seen, the model was able to predict the coefficients quite accurately on all aspects of the system's response.

In the first experiment ($V = 10$m/s and $\delta_c = 10°$) the scale model found an equilibrium after one second and two oscillations. During this experiment, the air flow remained attached to the wing until the initial stall, which occurred at approximately $\alpha = 17.0°$ and $\dot{\alpha} = 13.2°$/s. From this point, the model cycled through all the modes in 1.0s. The model was able to match this behavior, with the following GoFs: $GoF_{C_L} = 92.7\%$, $GoF_{C_D} = 60.2\%$, $GoF_{C_m} = 57.0\%$.

In the second experiment ($V = 10$m/s and $\delta_c = 20°$), three distinct behaviors can be seen. Firstly, the system followed the same behavior as in the previous experiment, with an attached airflow until an initial stall was encountered. In this experiment, stall occurred at $\alpha = 21.0°$ and $\dot{\alpha} = 112°$/s. After this initial stall, the system entered an oscillatory behavior, where it cycled through the modes seven times during 2.9s, at a frequency of about 2.5Hz. Finally, an equilibrium was found with the air flow detached. Once again, the model matched the experimental results, with the following GoFs: $GoF_{C_L} = 84.8\%$, $GoF_{C_D} = 74.1\%$, $GoF_{C_m} = 75.0\%$.

VI. CONCLUSION

In this paper, a new Hybrid Polynomial Stall Model (HPSM) was proposed for the modeling of the aerodynamic coefficients of a fixed-wing UAV including high angles of attack. In order to best model the aerodynamic hysteresis loop, it leveraged the capabilities of hybrid models to predict different values for the same abscissae depending on their mode. The HPSM features four such modes, two for attached and detached air flows respectively and two for the morphing from one to the other.

In addition, a method for the definition of identification constraints guaranteeing the continuity of the learned model was presented. Combined with the HPSM polynomial shape, it enabled the use of the Linearly Constrained Least Squares (LCLS) formulation for its identification, to which an analytical solution is known. This allows both for a quick and effortless offline identification and the possibility to optimize hyper-parameters, such as the constraint ones.

This solution was used in order to confront the model's prediction with experimental data from wind tunnel experiments. This comparison showcased Goodnesses of Fit as high as 80% using the NRMSE cost function, showing the model's precision.

Finally, this model requires only minimal knowledge of the specific aerodynamics of the airplane, enabling a widespread use. Moreover, its piecewise polynomial shape allows for the use of existing analysis and control tools, such as Sum of Squares (SoS) or Linear Fractional Transformation (LFT), which will be explored in future works.

REFERENCES

[1] A. Murch and J. Foster, "Recent nasa research on aerodynamic modeling of post-stall and spin dynamics of large transport airplanes," in *45th AIAA aerospace sciences meeting and exhibit*, 2007, p. 463.

[2] H. Hu, Z. Yang, and H. Igarashi, "Aerodynamic hysteresis of a low-reynolds-number airfoil," *Journal of Aircraft*, vol. 44, no. 6, pp. 2083–2086, 2007.

[3] D. Fischenberg, "Identification of an unsteady aerodynamic stall model from flight test data," in *20th Atmospheric Flight Mechanics Conference*, 1995, p. 3438.

[4] J. G. Leishman and T. Beddoes, "A semi-empirical model for dynamic stall," *Journal of the American Helicopter society*, vol. 34, no. 3, pp. 3–17, 1989.

[5] R. Jain, A. Le Pape, A. Grubb, M. Costes, F. Richez, and M. Smith, "High-resolution computational fluid dynamics predictions for the static and dynamic stall of a finite-span oa209 wing," *Journal of Fluids and Structures*, vol. 78, pp. 126–145, 2018.

[6] EU, "Commission implementing regulation (eu) 2019/947 of 24 may 2019 on the rules and procedures for the operation of unmanned aircraft (text with eea relevance)," *Official Journal of the European Union*, vol. 2019, May 2019.

[7] D. Keller, D. Farcy, and J.-F. Le Roy, "Numerical investigation of the aerodynamic behavior of a generic light aircraft," in *AAAF AERO2019*, 2019.

[8] D. Farcy, A. N. Khrabrov, and M. E. Sidoryuk, "Sensitivity of spin parameters to uncertainties of the aircraft aerodynamic model," *Journal of Aircraft*, vol. 57, no. 5, pp. 922–937, 2020.

[9] E. A. Morelli, K. Cunningham, and M. A. Hill, "Global aerodynamic modeling for stall/upset recovery training using efficient piloted flight test techniques," in *AIAA Modeling and Simulation Technologies (MST) Conference*, 2013, p. 4976.

[10] H. Tol, C. De Visser, L. Sun, E. van Kampen, and Q. Chu, "Multivariate spline-based adaptive control of high-performance aircraft with aerodynamic uncertainties," *Journal of Guidance, Control, and Dynamics*, vol. 39, no. 4, pp. 781–800, 2016.

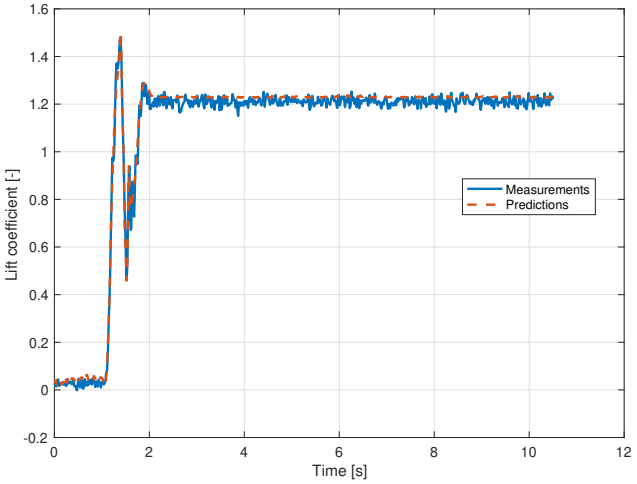

(a) Lift coefficient for $V = 10$m/s and $\delta_c = 10°$.

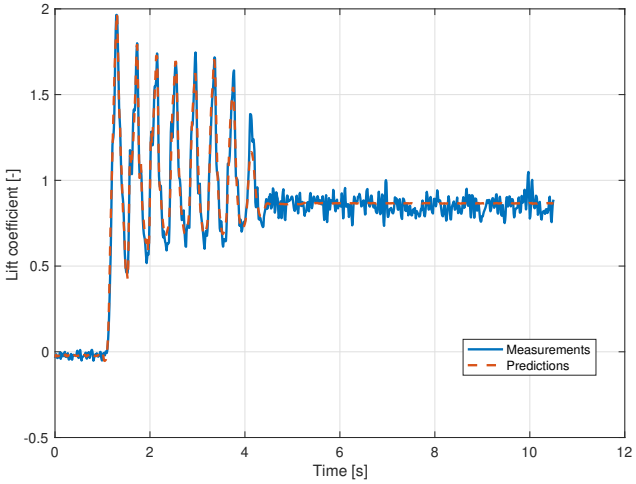

(b) Lift coefficient for $V = 10$m/s and $\delta_c = 20°$.

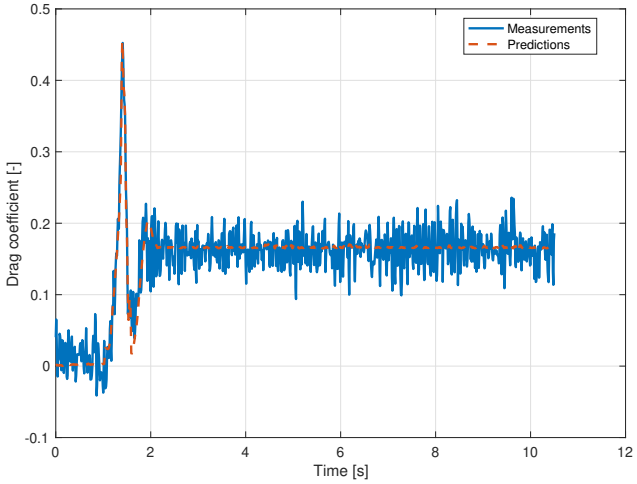

(c) Drag coefficient for $V = 10$m/s and $\delta_c = 10°$.

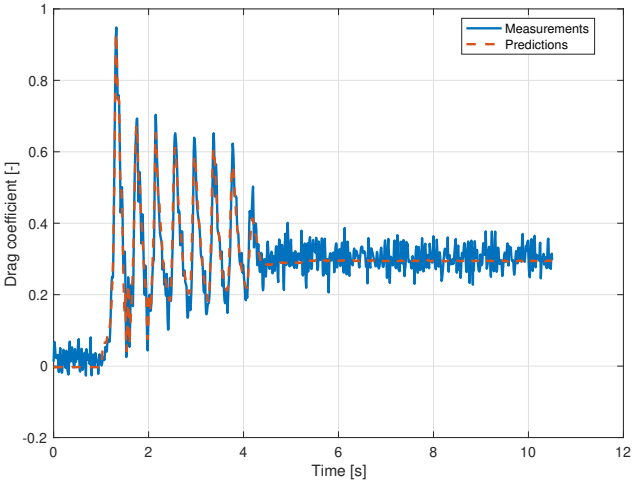

(d) Drag coefficient for $V = 10$m/s and $\delta_c = 20°$.

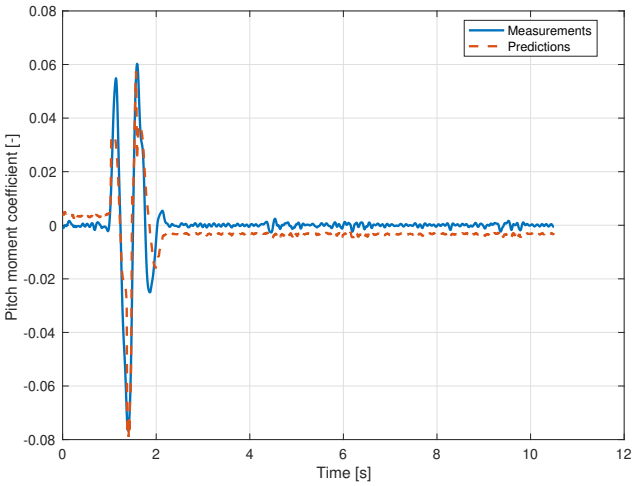

(e) Pitch moment coefficient for $V = 10$m/s and $\delta_c = 10°$.

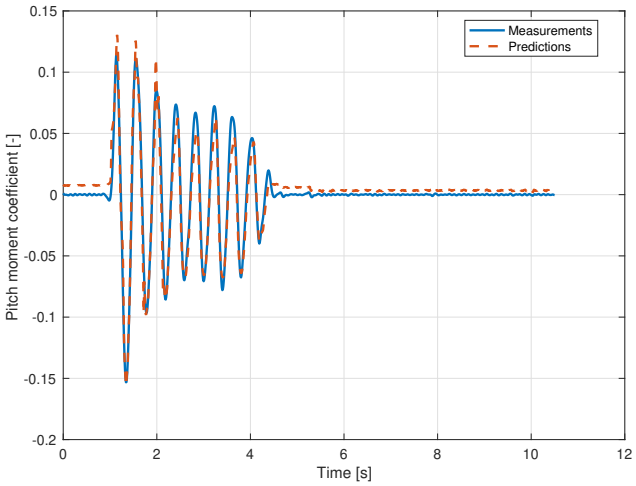

(f) Pitch moment coefficient for $V = 10$m/s and $\delta_c = 20°$.

Fig. 2. Measurements and predictions on each aerodynamic coefficient for two experiments.

[11] D. Greenwell, "A review of unsteady aerodynamic modelling for flight dynamics of manoeuvrable aircraft," in *AIAA atmospheric flight mechanics conference and exhibit*, 2004, p. 5276.

[12] A. R. Gallant and W. A. Fuller, "Fitting segmented polynomial regression models whose join points have to be estimated," *Journal of the American Statistical Association*, vol. 68, no. 341, pp. 144–147, 1973.

[13] V. M. Muggeo, "Estimating regression models with unknown break-points," *Statistics in medicine*, vol. 22, no. 19, pp. 3055–3071, 2003.

[14] N. Dong and J. Roychowdhury, "Piecewise polynomial nonlinear model reduction," in *Proceedings 2003. Design Automation Conference (IEEE Cat. No. 03CH37451)*. IEEE, 2003, pp. 484–489.

[15] C. Rabbath and D. Corriveau, "A comparison of piecewise cubic hermite interpolating polynomials, cubic splines and piecewise linear functions for the approximation of projectile aerodynamics," *Defence Technology*, vol. 15, no. 5, pp. 741–757, 2019.

[16] T. Cunis, L. Burlion, and J.-P. Condomines, "Piecewise polynomial modeling for control and analysis of aircraft dynamics beyond stall," *Journal of guidance, control, and dynamics*, vol. 42, no. 4, pp. 949–957, 2019.

[17] V. Guibert, J.-P. Condomines, M. Brunot, and M. Bronz, "Piecewise polynomial model identification using constrained least squares for uas stall," *IFAC-PapersOnLine*, vol. 54, no. 7, pp. 493–498, 2021.

[18] Sufendi, B. R. Trilaksono, S. H. Nasution, E. B. Purwanto, *et al.*, "Design and implementation of hardware-in-the-loop-simulation for uav using pid control method," in *2013 3rd International Conference on Instrumentation, Communications, Information Technology and Biomedical Engineering (ICICI-BME)*. IEEE, 2013, pp. 124–130.

[19] K. T. Borup, T. I. Fossen, and T. A. Johansen, "A machine learning approach for estimating air data parameters of small fixed-wing uavs using distributed pressure sensors," *IEEE Transactions on Aerospace and Electronic Systems*, vol. 56, no. 3, pp. 2157–2173, 2019.

[20] C. Roos, G. Hardier, and J.-M. Biannic, "Polynomial and rational approximation with the apricot library of the smac toolbox," in *2014 IEEE Conference on Control Applications (CCA)*. IEEE, 2014, pp. 1473–1478.

[21] P. J. Antsaklis, J. A. Stiver, and M. Lemmon, "Hybrid system modeling and autonomous control systems," in *Hybrid systems*. Springer, 1992, pp. 366–392.

[22] P. Stoica and Y. Selen, "Model-order selection: a review of information criterion rules," *IEEE Signal Processing Magazine*, vol. 21, no. 4, pp. 36–47, 2004.

[23] F. J. Solis and R. J.-B. Wets, "Minimization by random search techniques," *Mathematics of operations research*, vol. 6, no. 1, pp. 19–30, 1981.